Brief Communication

MOLECULAR METABOLISM

Mitochondrial disease disrupts hepatic allostasis and lowers the threshold for immune-mediated liver toxicity

Maxim Jestin [1,7], Senta M. Kapnick [1,7], Tatyana N. Tarasenko [1], Cassidy T. Burke [1], Patricia M. Zerfas [2], Francisca Diaz [3], Hilary Vernon [4], Larry N. Singh [5], Ronald J. Sokol [6], Peter J. McGuire [1,*,7]

ABSTRACT

Objective: In individuals with mitochondrial disease, respiratory viral infection can result in metabolic decompensation with mitochondrial hepatopathy. Here, we used a mouse model of liver-specific Complex IV deficiency to study hepatic allostasis during respiratory viral infection.
Methods: Mice with hepatic cytochrome c oxidase deficiency (*LivCox10*$^{-/-}$) were infected with aerosolized influenza, A/PR/8 (PR8), and euthanized on day five after infection following three days of symptoms. This time course is marked by a peak in inflammatory cytokines and mimics the timing of a common clinical scenario in which caregivers may first attempt to manage the illness at home before seeking medical attention. Metabolic decompensation and mitochondrial hepatopathy in mice were characterized by serum hepatic testing, histology, electron microscopy, biochemistry, metabolomics, and bioenergetic profiling.
Results: Following influenza infection, *LivCox10*$^{-/-}$ mice displayed marked liver disease including hepatitis, enlarged mitochondria with cristae loss, and hepatic steatosis. This pathophysiology was associated with viremia. Primary hepatocytes from *LivCox10*$^{-/-}$ mice cocultured with WT Kupffer cells in the presence of PR8 showed enhanced lipid accumulation. Treatment of hepatocytes with recombinant TNFα implicated Kupffer cell-derived TNFα as a precipitant of steatosis in *LivCox10*$^{-/-}$ mice. Eliminating Kupffer cells or blocking TNFα *in vivo* during influenza infection mitigated the steatosis and mitochondrial morphologic changes.
Conclusions: Taken together, our data shift the narrative of metabolic decompensation in mitochondrial hepatopathy beyond the bioenergetic costs of infection to include an underlying susceptibility to immune-mediated damage. Moreover, our work suggests that immune modulation during metabolic decompensation in mitochondrial disease represents a future viable treatment strategy needing further exploration.

Keywords Immunometabolism; Mitochondrial disease; Influenza; Viral infection; Kupffer cells; TNFα

1. INTRODUCTION

Mitochondrial diseases are a group of genetically and phenotypically heterogeneous disorders involving pathogenic variants in genes encoding proteins involved in oxidative phosphorylation (OXPHOS) and mitochondrial maintenance. With a minimum prevalence of 1 in 5,000, mitochondrial diseases represent some of the most common metabolic disorders presenting in childhood [1,2]. As mitochondria are ubiquitous, the clinical effects of mitochondrial disease are multisystemic, most significantly involving organs with large energy requirements such as the heart, brain, skeletal muscle, and liver.

From a clinical standpoint, one of the most challenging aspects of treating mitochondrial disease is metabolic decompensation, exacerbation of underlying mitochondrial dysfunction, which can lead to disease progression with a rapidly fatal course [3–5]. Allostasis is the process by which a system responds to stressors (e.g., infection). Unlike homeostasis, which is based on the principle of a setpoint, allostasis translates to "stability through change", where the setpoint may move. Allostatic mechanisms include stress responses, metabolic reprogramming, and even immunity, all of which occur at the cellular to the organismal level. Tissues affected by the mitochondrial disease have abnormal cell stress responses [6] and lower thresholds for drug toxicity [7], suggesting that metabolic decompensation in mitochondrial disease represents a failure of allostasis.

Treatment during metabolic decompensation in mitochondrial disease is primarily aimed at alleviating bioenergetic stress: (1) maintaining hydration, (2) providing calories, (3) correcting metabolic derangements, (4) avoiding mitochondrial toxins (i.e., drugs), (5)

[1]National Human Genome Research Institute, National Institutes of Health, Bethesda, MD, 20892, USA [2]Office of Research Services, National Institutes of Health, Bethesda, MD, 20892, USA [3]University of Miami, Department of Neurology, Miller School of Medicine, Miami, FL, 33136, USA [4]Kennedy Krieger Institute, Johns Hopkins Medical Center, Baltimore, MD, 21205, USA [5]Center for Mitochondrial and Epigenomic Medicine, Children's Hospital of Philadelphia, Philadelphia, PA, 19104, USA [6]Section of Pediatric Gastroenterology, Hepatology and Nutrition, University of Colorado School of Medicine and Children's Hospital Colorado, Aurora, CO 80045, USA

[7] Co-first authors/these authors contributed equally to this work.

*Corresponding author. National Human Genome Research Institute National Institutes of Health, 10 Center Drive, Room 7N260A Bethesda, MD, 20892, USA. E-mail: peter.mcguire@nih.gov (P.J. McGuire).

Received June 10, 2019 • Revision received March 3, 2020 • Accepted March 16, 2020 • Available online 26 March 2020

https://doi.org/10.1016/j.molmet.2020.100981

providing antioxidant/cofactor therapies, and (6) treating infections [4]. A viral infection is a known precipitant of metabolic decompensation in individuals with the mitochondrial disease [8,9], with 50% of the episodes being life-threatening or leading to serious sequelae [5]. Complicating matters further, up to 80% of children with mitochondrial disease experience recurrent or severe infections, most of which are respiratory viral infections [10]. Given the unavoidable risk of respiratory viral infection in children, there is a critical need to understand the mechanisms underlying metabolic decompensation to facilitate the development of therapies to reduce morbidity and mortality in patients with mitochondrial disease.

Given the limitations and varying success of therapies aimed at the bioenergetic costs of infection, here we address the specific relationship between immune activation and metabolic decompensation in the liver. Using a mouse model of mitochondrial hepatopathy and mouse-adapted influenza, we were able to recapitulate features of mitochondrial hepatopathy [8] due to COX deficiency. We show that Kupffer cell-derived TNFα can act as an endogenous mitochondrial toxin resulting in an exacerbation of mitochondrial function and disease progression marked by abnormal mitochondrial morphology, perturbations in lipid metabolism, and the development of steatohepatitis. Blocking the effects of TNFα ameliorated changes in mitochondrial morphology and development of hepatic steatosis in *LivCox10*$^{-/-}$ mice. Overall, livers affected by mitochondrial disease displayed a lower threshold for immune-mediated toxicity, illustrating a novel component of the pathophysiology of metabolic decompensation.

2. METHODS

2.1. Murine model of *LivCox10*$^{-/-}$

B6.129X1-Cox10^{tm1Ctm}*/J* mice (University of Miami, Miami, FL, USA) [11] were crossed with albumin-Cre transgenic mice B6.Cg-Speer6-ps1$^{Tg(Alb\text{-}cre)21Mgn}$/J (Jackson Laboratory, Bar Harbor, ME, USA) to produce a liver-specific *Cox10* knockout (*LivCox10*$^{-/-}$) mouse line. Both control and affected mice were maintained on a C57BL6/J background. The Cre-recombinase was maintained in the heterozygous state to produce healthy animals with the same life span as littermate controls [8]. In all experiments, 8-week-old mice (56 days) were used, a time point during which changes in mitochondrial morphology and lipid accumulation in the liver are not yet observed [8]. Mice were housed in a temperature (22 ± 2 °C) and humidity-controlled (30–70%) pathogen-free facility under a 12-hour light/dark cycle, with access to a 22% protein pellet-based feed (Bio-Serv, Frenchtown, NJ, USA) and autoclaved, reverse-osmosis water. All studies were approved by the Animal Care and Use Committee of the National Human Genome Research Institute.

2.2. A/PR/8/34 (PR8) infection and *in vivo* treatments

Mouse-adapted human influenza virus A/PR/8/34 (PR8) was used for all experiments, unless otherwise indicated (gift from Maryna Eichelberger). Mice were exposed to aerosolized PR8 (500 TCID50) in an inhalation apparatus (Glas-Col, Terre Haute, IN, USA) and euthanized five days after infection by CO_2 inhalation followed by cervical dislocation [12–14], in compliance with policies set forth by the Animal Care and Use Committee of the National Human Genome Research Institute. Tissues were collected, frozen, and stored at −80 °C until use. Liver-resident macrophages (Kupffer cells) were depleted prior to infection through intraperitoneal injection of liposome-encapsulated clodronate (0.2 mL, Clodrosome, Encapsula NanoSciences LLC, Brentwood, TN, USA). To block TNFα *in vivo*, mice received two doses of etanercept via intraperitoneal injection (100μg/dose, Immunex, Thousand Oaks, CA, USA) at the time of infection and 24 h after infection.

2.3. Biochemical parameters

Mice were anesthetized prior to collection to minimize stress responses. Blood was collected at the same time of day in the morning for each trial. Glucose level was determined using a standard handheld glucometer (Precision Xtra, Abbott Diabetes Care, Alameda, CA, USA) on the whole blood collected by retroorbital bleeding. Serum was separated from the whole blood, and serum aspartate aminotransferase (AST), total bilirubin, alkaline phosphatase (Alk Phos), and lactate were measured using dry-slide technology (VetTest 8008, IDEXX, Columbia, MO, USA).

2.4. Real-time quantitative PCR

DNA and RNA were extracted from homogenized tissue using a GeneJET Genomic DNA Kit and PureLink RNA Mini Kit (ThermoFisher), respectively. RT-qPCR reactions were carried out on StepOnePlus Real-Time PCR System (Applied Biosystems, Foster City, CA, USA) using SYBR Green PCR Master Mix (ThermoFisher). To evaluate gene expression, 1 μg of RNA was reverse-transcribed to cDNA using a modified MMLV-reverse transcriptase (iScript, Bio-Rad, Hercules, CA, USA). Virulence was determined by the relative detection of viral nonstructural protein (NS1) using real-time quantitative PCR (RT-qPCR) normalized to β-actin. The expression of the NS1 gene in lung samples was measured using the oligonucleotides primers: 5′-TTCACCATTGCCTTCTCTTC-3′ and 5′-CCCATTCTCATTACTGCTTC-3′, and β-actin primers: 5′-CCCTACAGTGCTGTGGGTTT-3′ and 5′-GAGACATGCAAGGAGTGCAA-3' (IDT DNA, Coralville, IA, USA).

2.5. Immunoblot

Protein was extracted from homogenized liver tissue using Tissue Protein Extraction Reagent (ThermoFisher Scientific, Waltham, MA, USA). 20 μg was loaded on a 4–20% Tris-glycine polyacrylamide gel, run at 120 V for 90 min under reducing conditions, and subsequently transferred to a nitrocellulose membrane using the Trans-Blot Turbo Transfer System (Bio-Rad, Hercules, CA, USA). Membranes were incubated in blocking buffer (Li-Cor Biosciences, Lincoln, NE, USA) for 1 h at 4 °C before incubation with the following primary antibodies overnight at 4 °C: HADHA (ab203114, Abcam, Cambridge, MA, USA), ACADVL (ab155138, Abcam, Cambridge, MA, USA), PPARα (ab126285, Abcam, Cambridge, MA, USA), and β-actin (A5441, Millipore Sigma, St. Louis, MO, USA). Membranes were washed three times for 10 min each with TBS+0.1% Tween-20 (Millipore Sigma, St. Louis, MO, USA), followed by incubation with the appropriate IRDye secondary antibody (IRDye® 800CW Goat anti-Rabbit IgG (H+L) (926–32211, Li-Cor Biosciences, Lincoln, ME, USA) and IRDye® 680LT Goat anti-Mouse IgG (H+L) (926–68020, Li-Cor Biosciences, Lincoln, ME, USA)). Images were acquired and analyzed on an Odyssey Imager (Li-Cor Biosciences, Lincoln, NE).

2.6. Histology

Histological tissue staining for COX/SDH and hematoxylin and eosin (H&E) (Histoserv, Germantown, MD, USA) and Oil Red O (ORO) (American Histo Labs, Gaithersburg, MD, USA) was performed using standard techniques. For COX/SDH, tissues are stained with both the electron donor 3,3′-diaminobenzidine (DAB) and the electron acceptor nitroblue tetrazolium. Under these conditions, mitochondrial cristae of cells with functional COX stain brown for the indamine product. Cells with dysfunctional COX are not saturated by the DAB product that, in turn, allows for visualization of the blue formazan product, a readout

for SDH activity [Ross, J Vis Exp, 2011]. *In vitro* staining of primary hepatocytes with ORO and H&E was performed as described in [15].

2.7. Lipidomic and acylcarnitine profile analysis

Liquid chromatography-mass spectrometry lipidomics was performed by the Lipidomics Core Facility at Wayne State University School of Medicine (https://lipidomics.wayne.edu/). For acylcarnitine analysis, liquid chromatography tandem mass spectrometry was performed on frozen liver samples homogenized in PBS by the Genetics Laboratory of the Kennedy Krieger Institute of Johns Hopkins Medical Center (https://www.kennedykrieger.org/patient-care/centers-and-programs/genetics-laboratories).

2.8. Isolation of hepatocytes

Hepatocytes were obtained using a two-step collagenase perfusion method described previously, with modifications [16]. Briefly, the liver was perfused with 0.02% EGTA-containing Mg^{2+}/Ca^{2+}-free PBS followed by a collagenase solution (50–100 U/mL, type 1, CLSH, Worthington Biochemical, Lakewood, NJ, USA) in DMEM supplemented with 15 mM HEPES, 1.8 mM $CaCl_2$, 1 g/L glucose, and antibiotics. The fibrous capsule of the digested liver was torn to release cells into DMEM/F12 + 10% FBS and filtered through a 70 μm cell strainer. The resulting cell suspension was washed three times with PBS until supernatant became clear. The hepatocyte pellet was resuspended in 40% Percoll (Sigma Aldrich, St. Louis, MO, USA), centrifuged at 850×*g* for 7 min, and washed with PBS, and the resulting pellet containing viable hepatocytes was collected for further analysis and culture.

2.9. Isolation of Kupffer cells

Following the initial centrifugation step to pellet hepatocytes, as described above, the supernatant containing nonparenchymal cells was collected in a fresh tube and centrifuged at 1350×*g* for 10 min. The resulting pellet was washed with ACK buffer to lyse RBCs, resuspended in 10 mL PBS, and layered on top of a 25/50% Percoll gradient. The gradient was subsequently centrifuged at 850×*g* for 15 min, no brake, and both intermediate fractions were collected, washed with PBS, and resuspended in DMEM/F12. Kupffer cells were further isolated using selective adherence, as described in [17].

2.10. Coculture and stimulation of primary mouse liver cells

Freshly isolated hepatocytes were seeded in a Matrigel-coated 24-well plate (Corning, Corning, NY, USA) at 1 × 10^5 cells/well in DMEM/F12 + 10% FBS for 2–3 h at 37 °C, 5% CO_2 until attachment was observed, after which serum-containing media were replaced with serum-free DMEM/F12 and hepatocytes were incubated overnight. 2 × 10^5 nonparenchymal cells were added to 24-well transwells; approximately 4 × 10^4 Kupffer cells after selective adherence. Adherent Kupffer cells were incubated overnight in DMEM/F12 + 10% FBS at 37 °C, 5% CO_2. After overnight incubation, transwells with adherent Kupffer cells were transferred to wells containing hepatocytes and cultured in the presence of PR8 in serum-free DMEM/F12 for 24 h. Cytokines were analyzed using a Cytometric Bead Array for mouse inflammatory markers on a FACSCalibur flow cytometer according to the manufacturer's instructions (BD Biosciences, San Jose, CA, USA).

2.11. Fluorescence microscopy

Plated hepatocytes and Kupffer cells were incubated with PR8-GFP (a gift from Dr. Adolfo Garcia-Sastre, Icahn School of Medicine, NY, NY, USA) in serum-free DMEM/F12 for 4 h at 37 °C, 5% CO_2, washed, and replaced with fresh media. To visualize for lysosomal structures, Kupffer cells were stained with 50 nM LysoTracker Red DND-99 (L7528, ThermoFisher Scientific, Rockville, MD, USA) in serum-free DMEM/F12 for 30 min at 37 °C, 5% CO_2. The loading solution was replaced with fresh media and cells were immediately imaged. Wide-field images were collected using an inverted Zeiss Axio Observer D1 microscope (Carl Zeiss Inc., Thornwood, NY, USA) with a dry Plan-Neofluar 40×/0.75 NA objective lens and an X-Cite metal halide lamp. All images were acquired using an AxioCam HRm CCD camera with a 1388 × 1040 pixel imaging field. DAPI, GFP, and LysoTracker Red were collected in emission filters 420–470, 515–565, and 593–668, respectively. Bright-field images were also collected. Zeiss ZEN Blue Pro 2011 software package was used for the acquisition of all images.

2.12. Transmission electron microscopy

Mouse livers (approximately 1 mm^3) were fixed in 2% glutaraldehyde in 0.1 M cacodylate buffer (pH 7.4) overnight at 4 °C and subsequently washed three times with cacodylate buffer. Tissues were fixed in 2% OsO_4 for 2 h, washed with cacodylate buffer three times, washed with water, and placed in 1% uranyl acetate for 1 h. Tissues were serially dehydrated in ethanol and propylene oxide and embedded in EMBed 812 resin (Electron Microscopy Sciences, Hatfield, PA, USA). Tissue sections of approximately 80 nm were obtained using the Leica Ultracut UCT Ultramicrotome (Leica, Deerfield, IL, USA), placed onto 300 mesh copper grids, and stained with saturated uranyl acetate in 50% methanol followed by lead citrate. Samples were viewed on the JEM-1200EXII electron microscope (JEOL Ltd, Tokyo, Japan) at 80 kV and imaged on the XR611M, mid-mounted, 10.5 Mpixel, CCD camera (Advanced Microscopy Techniques Corp, Danvers, MA, USA).

2.13. Patient data

Clinical data were abstracted from a chart review of the patient's medical history. Histology and electron microscopy were performed by the Children's Hospital Colorado and University of Colorado School of Medicine Department of Pathology.

2.14. Statistics

Statistical analyses were performed using GraphPad Prism (GraphPad Software, La Jolla, CA, USA) and Metaboanalyst 4.0 (https://www.metaboanalyst.ca/). *P* values less than 0.05 were considered statistically significant.

3. RESULTS

3.1. *LivCox10*$^{-/-}$ mice exhibit markers of enhanced hepatic injury following influenza infection

COX deficiency is one of the most common causes of mitochondrial hepatopathy in children [18]. Patients with mitochondrial hepatopathy due to COX deficiency [8] can present with marked hepatitis and liver dysfunction including hyperbilirubinemia, increased prothrombin time, hyperlactatemia, and steatosis (Fig. S1A). Given that viral infection is a known precipitant of metabolic decompensation in individuals with mitochondrial disease, we sought to investigate how respiratory viral infection exacerbates mitochondrial hepatopathy in mitochondrial disease due to Complex IV deficiency. To do this, we utilized a hepatocyte-targeted Cre-recombinase knockout of *Cox10* (*LivCox10*$^{-/-}$). *COX10* is an essential assembly factor required for cytochrome c oxidase (COX) function [19], the terminal respiratory complex responsible for the transfer of electrons from cytochrome c to oxygen. At eight weeks (56 days) of age, Complex IV activity was 84% reduced in hepatic lysates obtained from *LivCox10*$^{-/-}$ mice when compared with

LivCox10$^{+/+}$ littermates (Fig. S1B). This reduction is comparable to reductions of COX activity in patients with mitochondrial hepatopathy [20,21]. Likewise, livers isolated from *LivCox10*$^{-/-}$ mice showed staining for blue formazan product (Fig. S1C), confirming reduced COX enzyme activity. Although *LivCox10*$^{-/-}$ mice tended toward lower body weights when compared with *LivCox10*$^{+/+}$ littermates, this difference was not statistically significant (Fig. S1D). In addition, neither steatosis nor disruption of mitochondrial morphology was observed in liver sections examined via electron microscopy (Fig. S1E). Based on these data, we conclude that findings from the *LivCox10*$^{-/-}$ mouse model are consistent with the delayed-onset form of mitochondrial hepatopathy, making it suitable for exploring the role of infection in mitochondrial hepatopathy.

LivCox10$^{-/-}$ mice were infected with aerosolized mouse-adapted influenza A/PR/8 (PR8) and euthanized five days after infection. Mice are symptomatic between day three and day five, displaying reduced activity, ruffled fur, and decreased food intake. This timepoint mimics a common clinical presentation of metabolic decompensation, in which caregivers attempt to manage the illness at home before visiting a physician or the hospital [12]. *NS1,* a viral gene coding for the core structural protein of the PR8 virus, was measured in the lungs by RT-qPCR and was found to be comparable between *LivCox10*$^{+/+}$ and *LivCox10*$^{-/-}$, indicating similar susceptibility to viral infection (Figure 1A). Serum cytokine concentrations were also equivalent in infected *LivCox10*$^{+/+}$ and *LivCox10*$^{-/-}$ animals (Figure 1B). In contrast, *LivCox10*$^{-/-}$ lost more weight than *LivCox10*$^{+/+}$ littermates on days three and four (Figure 1C), indicating differences in morbidity associated with infection. Serum AST, Alk Phos, and total bilirubin were significantly increased in *LivCox10*$^{-/-}$ mice (Figures 1D), accompanied by decreased blood glucose levels (Figure 1E) on day five following PR8 infection. Disruption of glucose homeostasis is consistent with an impairment of hepatic function [22] and is often seen in patients with mitochondrial hepatopathy [18]. Because providing calories is a common treatment strategy for patients with mitochondrial disease [4], we performed pair-feeding experiments to eliminate potential effects of reduced food intake on blood glucose and liver function in PR8-infected *LivCox10*$^{-/-}$ when compared with littermate controls. Consistent with non-pair-fed mice, *LivCox10*$^{-/-}$ pair-fed mice exhibited significantly lower blood glucose levels and higher serum AST than *LivCox10*$^{+/+}$ mice (Fig. S2A). These data indicate that COX deficiency in the liver leading to hepatic injury following influenza infection is not necessarily due to reduced food intake by *LivCox10*$^{-/-}$ animals. Taken together, these findings establish 56-day-old *LivCox10*$^{-/-}$ mice as a suitable model for exploring the role of infection in precipitating hepatic disease in the context of Complex IV deficiency.

3.2. *LivCox10*$^{-/-}$ mice develop hepatitis steatosis in response to infection

Loss of COX activity and hepatic dysfunction following infection led us to look for changes in mitochondrial morphology that might be consistent with mitochondrial dysfunction [23]. Electron micrograph (EM) studies of liver tissue revealed grossly enlarged mitochondria and loss of cristae in *LivCox10*$^{-/-}$ livers, which was not seen in infected *LivCox10*$^{+/+}$ mice or in uninfected mice from either genotype (Figures 2A and S2B). Infected *LivCox10*$^{+/+}$ displayed a mild overall

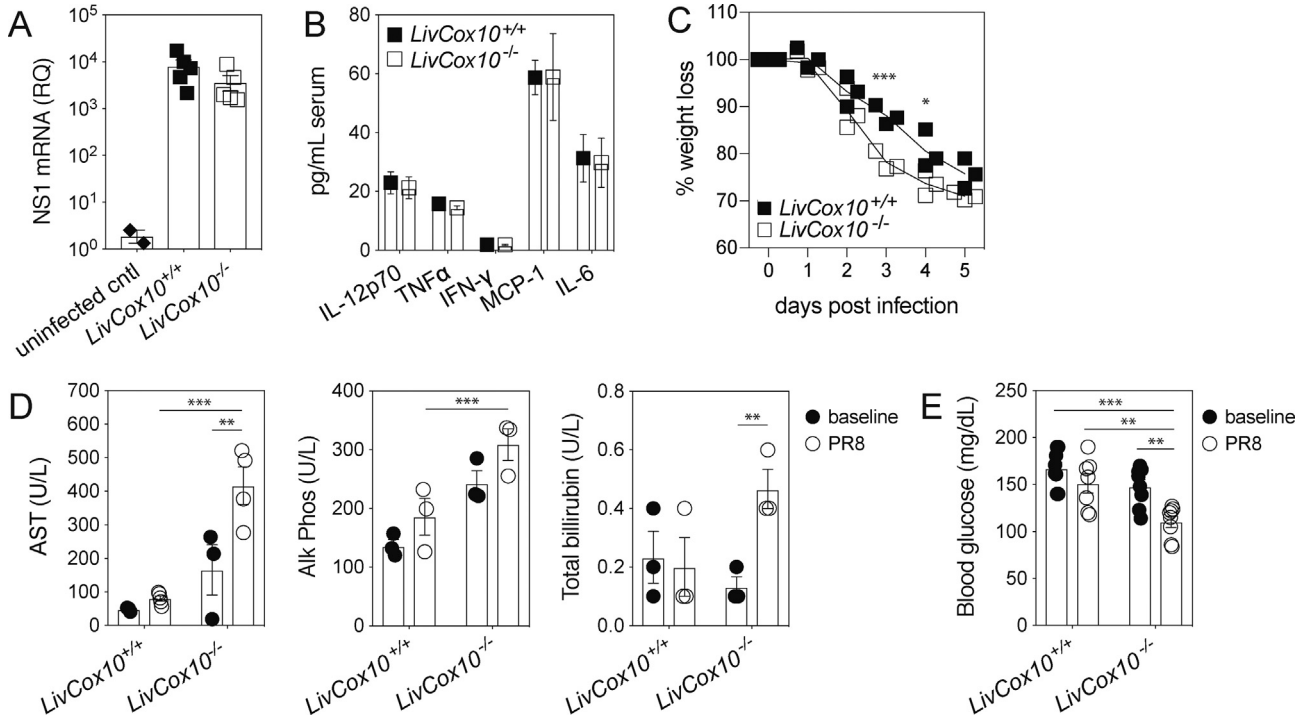

Figure 1: Influenza infection results in increased hepatic stress in *LivCox10*$^{-/-}$ mice. (A) RT-qPCR-based detection of the viral gene, NS1, in the lung five days after PR8 infection. $N = 2$ uninfected or 5 infected mice/group. (B) Serum cytokines measured by bead array five days after PR8 infection. IL-12p70: interleukin-12, active heterodimer; TNFα: tumor necrosis factor alpha; IFN-γ: interferon gamma; MCP-1: macrophage chemotactic protein 1; IL-6: interleukin 6. Data represent mean ± SEM. $N = 7$ mice/group. (C) Percent weight loss in mice during PR8 infection. $N = 3$ mice/group. Data are representative of two experiments. (D) Serum AST (left panel), Alk Phos (middle panel), and total bilirubin (right panel) in uninfected (closed circles) and PR8-infected (open circles) mice. $N = 3$–5 mice/group. (E) Blood glucose in uninfected (closed circles) and PR8-infected (open circles) mice. $N = 7$–8 mice/group. $^*P < 0.05$, $^{**}P < 0.01$, and $^{***}P < 0.001$.

increase in mitochondria size but could not be quantified due to the lack of volumetric data from EM images [24]. Furthermore, livers from infected *LivCox10*$^{-/-}$ also had a pronounced accumulation of lipid droplets (Figure 2A). ORO staining of sectioned livers from *LivCox10*$^{-/-}$ confirmed widespread steatosis in response to infection (Figures 2B and S2C).

Enhanced glycolysis is a known consequence of mitochondrial disease due to the inability to utilize OXPHOS for ATP production [25]. Pyruvate, the product of glycolysis, can either be reduced to lactate or converted to acetyl-CoA in the mitochondrial matrix, which serves as a precursor for fatty acid synthesis (FAS) following transport to the cytosol via a citrate intermediate (Fig. S2D). To test whether increased glycolysis in COX-deficient hepatocytes could lead to excessive lipid accumulation, we crossed *LivCox10*$^{-/-}$ mice to hepatocyte-targeted pyruvate dehydrogenase (*PDH*) knockout mice to generate *LivCox10*$^{-/-}$*PDH*$^{-/-}$ double knockout mice (DKO). Following PR8 infection, PDH deficiency abrogated lipid accumulation described above (Figure 2C), suggesting that steatosis in *LivCox10*$^{-/-}$ mice was being driven by de novo FAS as a result of increased glycolysis rather than increased lipid uptake.

Steatosis can result from a disruption of fatty acid oxidation (FAO), which also occurs in mitochondrial disease [26,27]. Since mitochondria are the ultimate acceptors of reducing equivalents generated from FAO [28], we hypothesized that a further deterioration in mitochondrial function due to infection would lead to impaired FAO and contribute to the accumulation of triacylglycerides in COX-deficient hepatocytes. To test this, we first characterized the triacylglycerides accumulating in *LivCox10*$^{-/-}$ livers using lipidomic analysis. In livers harvested from PR8-infected *LivCox10*$^{-/-}$ mice, we observed the predominantly long-chain fatty acid species, C16—C18 (Fig. S3A). Proliferator-activated receptor alpha (PPARα) is a positive regulator of FAO [29]; therefore, we examined PPARα expression in livers harvested from *LivCox10*$^{-/-}$ and *LivCox10*$^{+/+}$ mice at baseline and after PR8 infection. The expression of PPARα was similar in *LivCox10*$^{+/+}$ and *LivCox10*$^{-/-}$ mice at baseline and unchanged in *LivCox10*$^{+/+}$ livers before and after infection. In contrast, *LivCox10*$^{-/-}$ livers exhibited significantly increased PPARα expression after infection (Figures 2D and S3B). Very long-chain acyl-CoA dehydrogenase (ACADVL), an enzyme involved in long-chain FAO, similarly increased in *LivCox10*$^{-/-}$ livers after

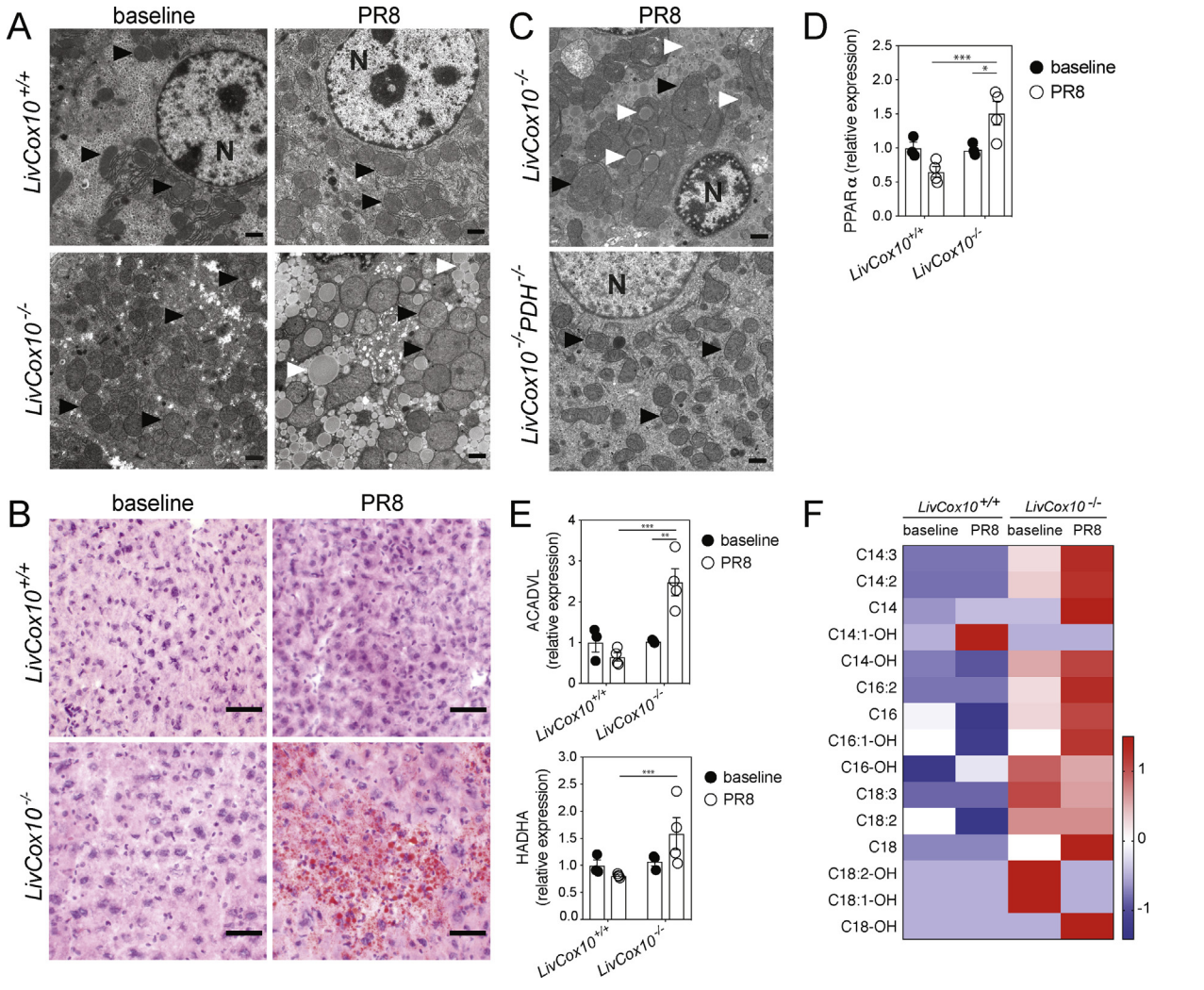

Figure 2: Hepatic steatosis in *LivCox10*$^{-/-}$ livers after influenza infection. (A) Representative EMs of livers isolated from uninfected mice (left column) or after PR8 infection (right column). Black arrows indicate mitochondria. White arrows indicate lipid. N: nucleus. Scale bar = 1 μm. $N = 4$ mice/group. Data are representative of three experiments. (B) Representative ORO stains of liver tissue prepared from uninfected (right column) or PR8-infected mice. Scale bar = 50 μm. $N = 4$ mice/group. Data are representative of three experiments. (C) Expression of PPARα protein in lysates prepared from liver tissue harvested from uninfected (solid circles) or PR8-infected (open circles) *LivCox10*$^{+/+}$ and *LivCox10*$^{-/-}$ mice. $N = 3$–4 mice/group. (D) Expression of ACADVL (top) and HADHA (bottom) proteins in liver lysates. $N = 3$–4 mice/group. (E) Heatmap of z-scores from acylcarnitine analyses of livers. $N = 8$ mice/group. Data represent mean ± SEM. $^*P < 0.05$, $^{**}P < 0.01$, and $^{***}P < 0.001$.

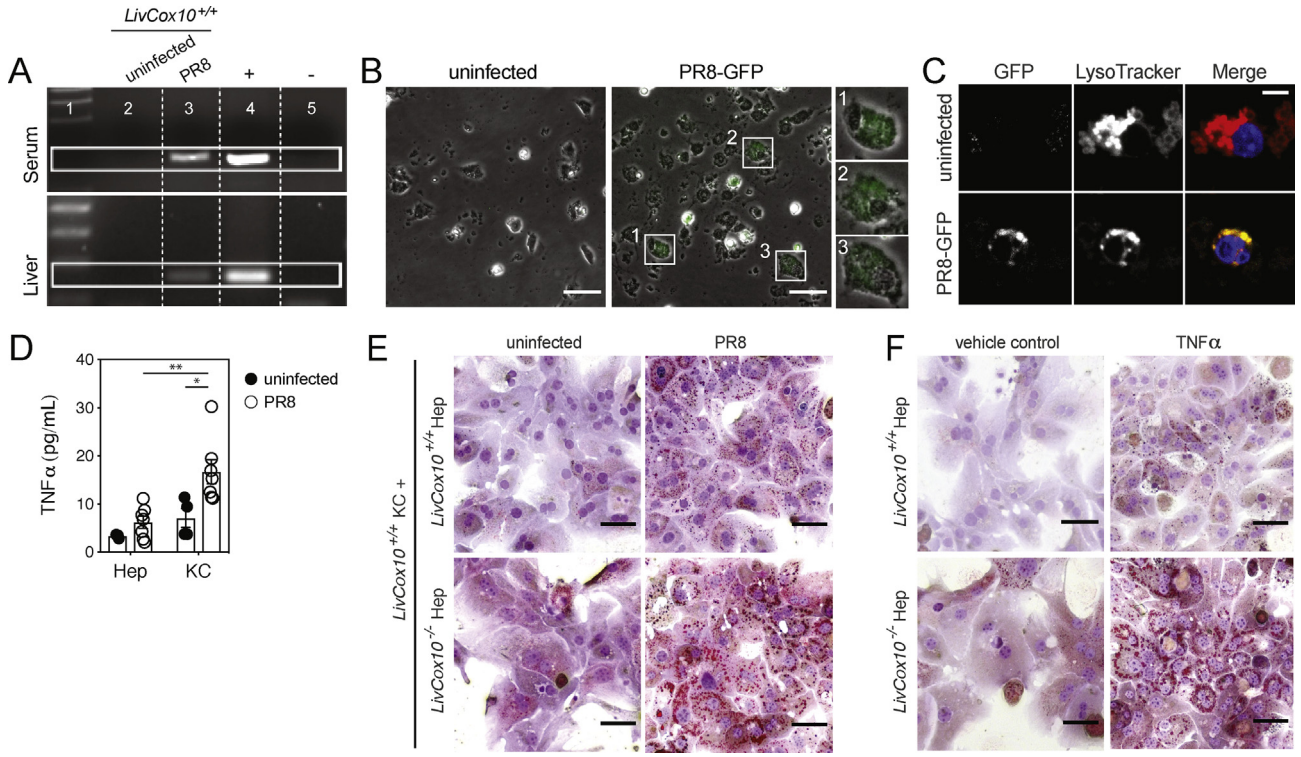

Figure 3: Kupffer cells promote lipid accumulation in *LivCox10*$^{-/-}$ hepatocytes in the presence of PR8 influenza. (A) RT-qPCR-based detection of NS1 in the serum and liver of *LivCox10*$^{+/+}$ mice. Lane 1: ladder; lane 2: uninfected *LivCox10*$^{+/+}$; lane 3: PR8-infected *LivCox10*$^{+/+}$; lane 4: positive control; lane 5: negative control. (B) Image of *in vitro* cultured *LivCox10*$^{+/+}$ Kupffer cells incubated for 24 h with PR8-GFP virus. Scale bar = 20 μm. Data are representative of two experiments. (C) Image of *LivCox10*$^{+/+}$ Kupffer cells incubated with PR8-GFP and counter-stained with LysoTracker. Left panel: PR8-GFP; middle panel: LysoTracker; right panel: merged image. Data are representative of two experiments. (D) TNFα concentration as measured by bead array in the supernatant of cultured *LivCox10*$^{+/+}$ hepatocytes (Hep) or Kupffer cells (KCs) in the absence or presence of PR8. Data represent mean ± SEM. (E) ORO-stained *LivCox10*$^{+/+}$ or *LivCox1*$^{-/-}$ Hep cocultured with *LivCox10*$^{+/+}$ KCs in the absence (left column) or presence (right column) of PR8. Scale bar = 50 μm. Data are representative of three experiments. (F) ORO-stained hepatocytes (Hep) cultured for 24 h in the presence of TNFα (20 ng/mL). Scale bar = 50 μm. Data are representative of three experiments. $^{*}P < 0.05$ and $^{**}P < 0.01$.

infection while *LivCox10*$^{+/+}$ exhibited no change after PR8 infection (Figures 2E and S3B). Hydroxyacyl CoA dehydrogenase (HADHA) was elevated in *LivCox10*$^{-/-}$ over *LivCox10*$^{+/+}$ mice after infection only (Figures 2E and S3B). Mass spectrometry revealed increased C16–C18 carnitine esters in livers harvested from uninfected *LivCox10*$^{-/-}$ mice, many of which further increased after infection in *LivCox10*$^{-/-}$ animals only (Figure 2F). These data show that the development of hepatic steatosis in mitochondrial hepatopathy also coincides with an impairment in long-chain FAO. Of note, steatosis could serve as a nidus for lipid peroxidation, further contributing to hepatic damage [30].

3.3. Kupffer cell activation during influenza infection promotes steatosis in *LivCox10*$^{-/-}$ hepatocytes

Having demonstrated a clear association between PR8 infection and exacerbation of mitochondrial hepatopathy over baseline in mice with deficient COX activity in the liver, we next sought to explore the mechanisms linking respiratory viral infection and hepatotoxicity. Previous studies showed that hepatic damage was dependent upon memory T-cell responses [31]. However, in the absence of an immune priming event, our scenario suggested the involvement of innate immune activation. During the course of PR8 infection, Kupffer cells expand and become activated [14]. These resident macrophages can modulate hepatic metabolism [14,32] and play an integral role in hepatic toxicity and steatosis [33–36]. Based on this, we hypothesized that Kupffer cells play a role in respiratory viral infection-initiated hepatotoxicity in our mouse model of liver-specific mitochondrial disease. Consistent with previous reports indicating a viremic spread of PR8 [37,38], the viral genome was detected by RT-qPCR in both serum and perfused liver tissue from *LivCox10*$^{+/+}$-infected mice (Figure 3A). To test whether Kupffer cells were able to take up viral particles and produce inflammatory cytokines, we incubated Kupffer cells isolated from *LivCox10*$^{+/+}$ livers in the presence of a recombinant PR8 virus expressing a green fluorescent protein reporter (PR8-GFP). Intracellular GFP was detected via microscopy in primary Kupffer cells incubated with PR8-GFP for 24 h (Figure 3B). Furthermore, GFP expression was found to colocalize with a lysosomal dye (Figure 3C), suggesting that viral particles had been phagocytosed. New viral particles were not detected in the media after three days of incubation (data not shown), suggesting that PR8-GFP was undergoing abortive replication in Kupffer cells. Intracellular PR8-GFP was not found in primary hepatocytes cultured in the presence of the virus under the same conditions (Fig. S4). Therefore, we conclude that Kupffer cells exposed *in vitro* to PR8-GFP are capable of viral uptake.

Hepatocytes and Kupffer cells share an intimate space in the liver, establishing a microenvironment for complex and dynamic interactions via intercellular signaling [39]. We hypothesized that cytokines released by Kupffer cells can contribute to the hepatotoxicity in our mouse model. To test this, we assembled a coculture in which primary hepatocytes and Kupffer cells were physically separated by a transmembrane and incubated in the presence of PR8-GFP. Cytokine analysis of the supernatant from Kupffer cells exposed to virus showed

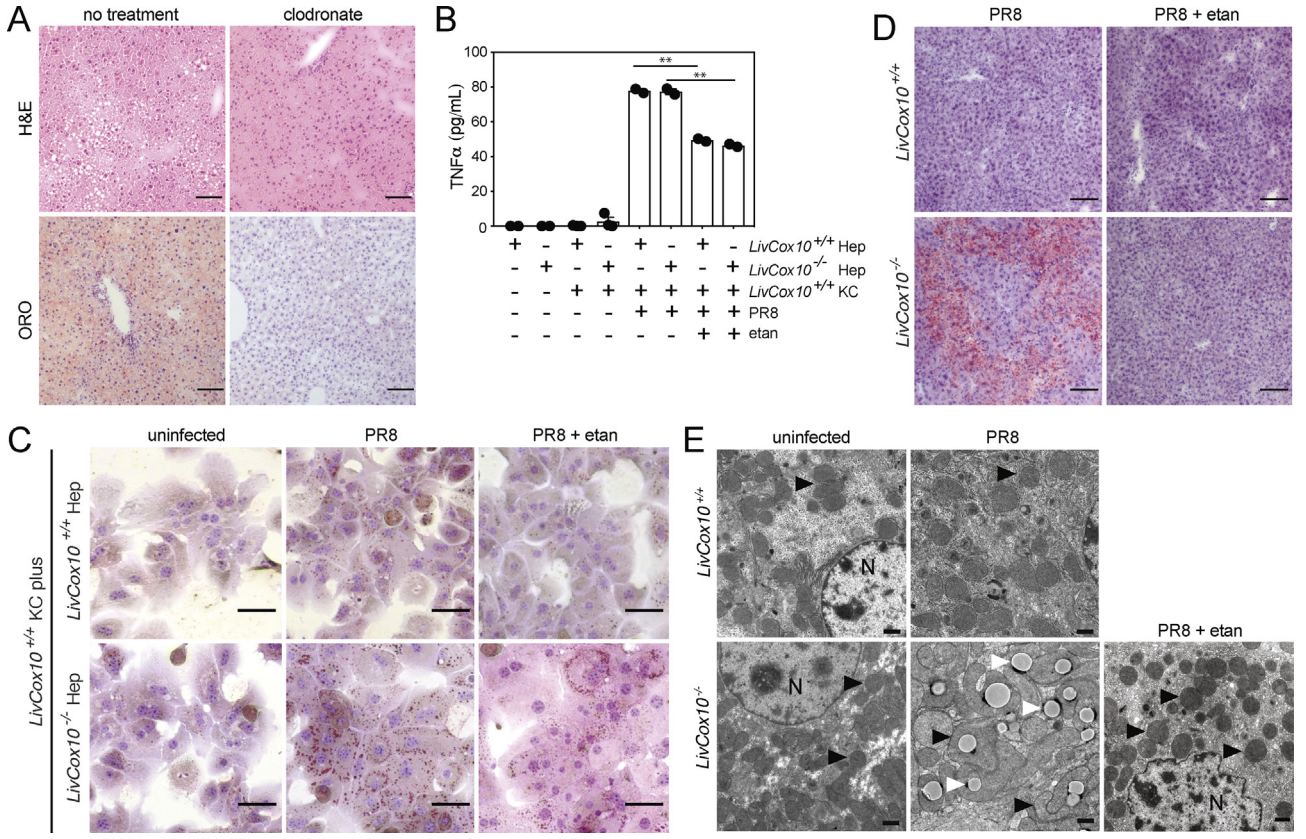

Figure 4: Treatment of *LivCox10*$^{-/-}$ mice with etanercept alleviates steatosis and abnormalities in mitochondrial morphology after the PR8 influenza infection. (A) Image of H&E and ORO-stained livers prepared from PR8-infected *LivCox10*$^{-/-}$ mice after treatment with clodronate. N = 3–4 mice/group. Data are representative of two experiments. Scale bar = 100 μm. (B) Detection of TNFα via bead array in the supernatant of *LivCox10*$^{+/+}$ or *LivCox10*$^{-/-}$ primary Hep cocultured with *LivCox10*$^{+/+}$ KCs exposed for 24 h to PR8-GFP (PR8) in the presence or absence of etanercept (etan). Data are representative of two experiments. Data represent mean ± SEM. $^{**}P < 0.01$. (C) Image of ORO-stained hepatocytes (Hep) after 24 h of coculture with KCs in the presence of PR8 and with or without etanercept. Scale bar = 50 μm. Data are representative of three experiments. (D) Image of ORO-stained liver tissue from PR8-infected mice treated with etanercept (etan). Scale bar = 100 μm. *N* = 3–4 mice/group. Data are representative of two experiments. (E) EMs of liver tissue from uninfected, PR8-infected, and PR8-infected *LivCox10*$^{+/+}$ or *LivCox10*$^{-/-}$ mice treated with etanercept (etan). *N* = 3–4 mice/group. Data are representative of 2 experiments. Black arrows indicate mitochondria. White arrows indicate lipids. Scale bar = 1 μm.

elevated TNFα (Figure 3D), a known proinflammatory and hepatotoxic cytokine involved in hepatic steatosis [40]. In the presence of PR8-GFP, *LivCox10*$^{-/-}$ hepatocytes cocultured with *LivCox10*$^{+/+}$ Kupffer cells showed more pronounced intracellular lipid deposition via ORO staining when compared to *LivCox10*$^{+/+}$ hepatocytes cocultured with *LivCox10*$^{+/+}$ Kupffer cells (Figure 3E). To determine if Kupffer cell-derived TNFα was driving lipid deposition in hepatocytes in our coculture system, we exposed *LivCox10*$^{+/+}$ and *LivCox10*$^{-/-}$ hepatocytes directly to recombinant TNFα for 24 h and stained with ORO. While *LivCox10*$^{+/+}$ hepatocytes showed mild lipid accumulation, *LivCox10*$^{-/-}$ hepatocytes demonstrated marked lipid deposition (Figure 3F). We conclude that TNFα plays a direct role in the development of hepatic steatosis in *LivCox10*$^{-/-}$ mice and that this is mediated in part via Kupffer cells after infection.

3.4. Modulation of TNFα during influenza infection mitigates hepatic steatosis and prevents aberrant mitochondrial morphology in *LivCox10*$^{-/-}$ mice

Our *in vitro* evidence demonstrating a role for Kupffer cells in the steatosis observed in COX-deficient hepatocytes led us to hypothesize that depleting Kupffer cells *in vivo* would ameliorate the steatosis phenotype observed during influenza infection. We delivered clodronate-containing liposomes via intraperitoneal injection to mediate *in vivo* depletion of the Kupffer cell population [41], followed by PR8 infection. Clodronate treatment reduced the hepatic steatosis observed in livers harvested from infected *LivCox10*$^{-/-}$ mice, as seen by H&E and ORO staining (Figure 4A). These data support a role for Kupffer cells in exacerbating mitochondrial hepatopathy in COX-deficient mice.

The knockdown of TNFα expression in myeloid cells has been reported to successfully diminish steatosis in a mouse model of nonalcoholic steatohepatitis (NASH) [42], suggesting that targeting this cytokine *in vivo* may also be beneficial in our model system. Etanercept is a soluble TNFα decoy receptor commonly used for the treatment of inflammatory diseases in humans [43] and previously shown to downregulate inflammatory immune responses providing protection against lethal influenza infection in mice [44]. Adding etanercept to hepatocytes isolated from *LivCox10*$^{+/+}$ and *LivCox10*$^{-/-}$ mice and cocultured with *LivCox10*$^{+/+}$ Kupffer cells in the presence of PR8 lowered TNFα in supernatants by 40% (Figure 4B) and also reduced the intensity of ORO staining (Figure 4C). These data further bolster the role of TNFα in lipid accumulation in *LivCox10*$^{-/-}$ hepatocytes but not WT cells during exposure to PR8. Based on these data, we hypothesized that etanercept could also attenuate the progression to steatosis in *LivCox10*$^{-/-}$ mice infected with PR8. To test this, *LivCox10*$^{-/-}$ mice were treated with etanercept the day of infection and 24 h after PR8

infection. Histological evaluation of livers five days after infection showed that etanercept successfully mitigated steatosis (Figure 4D) as well as reducing the presence of grossly enlarged mitochondria observed in liver EMs (Figure 4E). Thus, during influenza infection, Kupffer cells and TNFα can mediate both the progression of hepatopathy to steatosis and the development of the abnormal mitochondrial morphology in livers of *LivCox10*$^{-/-}$ mice.

4. CONCLUSIONS

Our model demonstrates that Kupffer cell-derived TNFα can serve as an endogenous toxin linking respiratory infection and mitochondrial hepatopathy in mitochondrial disease. While mitochondrial toxicity due to inflammatory cytokines has been reported [45] notably under extreme circumstances (e.g., sepsis) [45–49], we show here that COX-deficient hepatocytes displayed increased sensitivity to recombinant TNFα at concentrations that did not produce hepatitis or impact mitochondrial morphology in hepatocytes from *LivCox10*$^{+/+}$ mice. This suggests that tissues affected by Complex IV deficiency have a lower threshold for immune-mediated toxicity, a feature that has not been previously reported in mitochondrial disease. In light of this, it would be interesting to bypass Complex IV deficiency using an alternative oxidase (AOX) [50] to restore hepatic allostasis in *LivCox10*$^{-/-}$ mice.

Loss of COX activity in hepatocytes results in decreased oxygen consumption, lowered NAD^+/NADH ratios, reduction in reactive oxygen species (data not shown), and depleted glycogen with normal ATP production [11]. Taken together, these findings are consistent with reports describing increased reliance upon glycolysis in mitochondrial disease [25]. During the influenza challenge, the energy deficit due to a depression of OXPHOS enhances this reliance upon glycolysis, as evidenced by decreased serum glucose (i.e., increased glucose utilization) in PR8-infected *LivCox10*$^{-/-}$ mice during both non-pair-fed and pair-fed conditions. Since gluconeogenesis and glycolysis are reciprocally regulated in the liver, we propose that gluconeogenesis is also compromised in hepatocytes from *LivCox10*$^{-/-}$ mice. Furthermore, we report impaired FAO via acylcarnitine profile analysis, suggesting that glucose sparing by FAO (i.e., Randle cycle) is also dysfunctional. In addition to these cell-autonomous defects in COX-deficient hepatocytes, the effects of inflammation also need to be considered. Our previous work demonstrates metabolic reprogramming to glycolysis in healthy hepatocytes in response to inflammation during influenza infection [32]. While we cannot rule out the contribution of malic enzyme activity (cytosolic ME1 or mitochondrial ME2) contributing to the pyruvate pool, our hypothesis that the substrates for FAS are glycolytic in origin is consistent with the increase in glycolytic flux seen in mitochondrial disease [25] and during infection in hepatocytes [32]. Nevertheless, our data indicate that the source of the lipid accumulation is pyruvate, as indicated by our *Cox10/PDH* DKO data. Besides pyruvate, a potential source of citrate is via the reductive carboxylation of α-ketoglutarate [51,52] that occurs under conditions of depressed OXPHOS [53]. However, the work by our group found that, in the setting of COX deficiency in T cells, reductive carboxylation does not occur, as measured by isotopomer enrichment studies [10]. Moreover, if reductive carboxylation is critical for the accumulation of fat in COX-deficient hepatocytes, steatosis would remain in our *Cox10/PDH* DKO mice. Part of the plasticity of PDH-deficient cells involves reductive carboxylation where glutamine-derived acetyl-CoA is used for FAS [54]. Therefore, we speculate that in COX-deficient hepatocytes, pyruvate is converted to mitochondrial acetyl-CoA via PDH and enters the tricarboxylic acid (TCA) cycle where citrate is generated. That citrate is transported to the cytosol and converted to acetyl-CoA for FAS. Taken together, our findings offer insight into the metabolic mechanism driving steatosis in COX-deficient hepatocytes.

Interestingly, lipid accumulation and enlarged mitochondria during influenza infection in *LivCox10*$^{-/-}$ mice can be modulated by the administration of the anti-TNFα biologic, etanercept. While the administration of etanercept is not currently advisable for the treatment of hepatic steatosis in mitochondrial disease patients [55], our studies provide proof of principle that immune modulation represents a potentially novel approach to the problem of metabolic decompensation. In other words, the increasing availability of immunomodulatory biologics and drugs or alternate dosage may enable their use in future preclinical studies and represent a novel strategy to treat the cause of metabolic decompensation as opposed to the symptoms. Importantly, our studies expand the dialogue in mitochondrial medicine by focusing on the contributions of the immune system, a target that offers many opportunities for treatment in a disease that does not have many therapeutic options.

AUTHORS' CONTRIBUTIONS

The concept was contributed by M. J., S. M. K., T. N. T., and P. J. M. The analysis and investigation were done by M. J., S. M. K., C. T. B., T. N. T., P. M. Z., F. D., H. V., L. N. S., and P. J. M. The paper was written by M. J., S. M. K., and P. J. M. Reviewing and editing of the paper were done by S. M. K., T. N. T., C. T. B., and P. J. M.

ACKNOWLEDGEMENTS

The authors thank the Animal Core Facility at NHGRI for their support. This work was supported by the Intramural Research Program of the National Institutes of Health. Special thanks are due to Dr. Adolfo Garcia-Sastre for the PR8-GFP influenza virus, Dr. Maryna Eichelberger for the PR8 influenza virus, and Dr. Les Biesecker for reviewing the paper.

CONFLICTS OF INTEREST

The authors have declared that no conflicts of interest exist.

APPENDIX A. SUPPLEMENTARY DATA

Supplementary data to this article can be found online at https://doi.org/10.1016/j.molmet.2020.100981.

REFERENCES

[1] Ng, Y.S., Turnbull, D.M., 2016. Mitochondrial disease: genetics and management. Journal of Neurology 263(1):179–191.

[2] Thorburn, D.R., 2004. Mitochondrial disorders: prevalence, myths and advances. Journal of Inherited Metabolic Disease 27(3):349–362.

[3] Lee, W.S., Sokol, R.J., 2013. Mitochondrial hepatopathies: advances in genetics, therapeutic approaches, and outcomes. The Journal of Pediatrics 163(4):942–948.

[4] Parikh, S., Saneto, R., Falk, M.J., Anselm, I., Cohen, B.H., Haas, R., et al., 2009. A modern approach to the treatment of mitochondrial disease. Current Treatment Options in Neurology 11(6):414–430.

[5] Edmonds, J.L., Kirse, D.J., Kearns, D., Deutsch, R., Spruijt, L., Naviaux, R.K., 2002. The otolaryngological manifestations of mitochondrial disease and the risk of neurodegeneration with infection. Archives of Otolaryngology - Head and Neck Surgery 128(4):355–362.

[6] Suomalainen, A., 2011. Therapy for mitochondrial disorders: little proof, high research activity, some promise. Seminars in Fetal and Neonatal Medicine 16(4):236—240.
[7] Finsterer, J., Segall, L., 2010. Drugs interfering with mitochondrial disorders. Drug and Chemical Toxicology 33(2):138—151.
[8] Cormier-Daire, V., Chretien, D., Rustin, P., Rotig, A., Dubuisson, C., Jacquemin, E., et al., 1997. Neonatal and delayed-onset liver involvement in disorders of oxidative phosphorylation. The Journal of Pediatrics 130(5):817—822.
[9] Kisler, J.E., Whittaker, R.G., McFarland, R., 2010. Mitochondrial diseases in childhood: a clinical approach to investigation and management. Developmental Medicine and Child Neurology 52(5):422—433.
[10] Tarasenko, T.N., Pacheco, S.E., Koenig, M.K., Gomez-Rodriguez, J., Kapnick, S.M., Diaz, F., et al., 2017. Cytochrome c oxidase activity is a metabolic checkpoint that regulates cell fate decisions during T cell activation and differentiation. Cell Metabolism 25(6):1254—1268 e7.
[11] Diaz, F., Garcia, S., Hernandez, D., Regev, A., Rebelo, A., Oca-Cossio, J., et al., 2008. Pathophysiology and fate of hepatocytes in a mouse model of mitochondrial hepatopathies. Gut 57(2):232—242.
[12] McGuire, P.J., Tarasenko, T.N., Wang, T., Levy, E., Zerfas, P.M., Moran, T., et al., 2014. Acute metabolic decompensation due to influenza in a mouse model of ornithine transcarbamylase deficiency. Disease Models & Mechanisms 7(2):205—213.
[13] Tarasenko, T.N., Cusmano-Ozog, K., McGuire, P.J., 2018. Tissue acylcarnitine status in a mouse model of mitochondrial beta-oxidation deficiency during metabolic decompensation due to influenza virus infection. Molecular Genetics and Metabolism 125(1-2):144—152.
[14] Tarasenko, T.N., Singh, L.N., Chatterji-Len, M., Zerfas, P.M., Cusmano-Ozog, K., McGuire, P.J., 2015. Kupffer cells modulate hepatic fatty acid oxidation during infection with PR8 influenza. Biochimica et Biophysica Acta 1852(11):2391—2401.
[15] Mehlem, A., Hagberg, C.E., Muhl, L., Eriksson, U., Falkevall, A., 2013. Imaging of neutral lipids by oil red O for analyzing the metabolic status in health and disease. Nature Protocols 8(6):1149—1154.
[16] Zhang, W.. Primary hepatocyte isolation. 2010 6/2016]. Available from: http://mouselivercells.com/Documents/Hepatocyte%20Isolation%20Protocol.pdf.
[17] Smedsrod, B., Pertoft, H., Eggertsen, G., Sundstrom, C., 1985. Functional and morphological characterization of cultures of Kupffer cells and liver endothelial cells prepared by means of density separation in Percoll, and selective substrate adherence. Cell and Tissue Research 241(3):639—649.
[18] Lee, W.S., Sokol, R.J., 2007. Mitochondrial hepatopathies: advances in genetics and pathogenesis. Hepatology 45(6):1555—1565.
[19] Diaz, F., 2010. Cytochrome c oxidase deficiency: patients and animal models. Biochimica et Biophysica Acta 1802(1):100—110.
[20] Valnot, I., Osmond, S., Gigarel, N., Mehaye, B., Amiel, J., Cormier-Daire, V., et al., 2000. Mutations of the SCO1 gene in mitochondrial cytochrome c oxidase deficiency with neonatal-onset hepatic failure and encephalopathy. The American Journal of Human Genetics 67(5):1104—1109.
[21] Stiburek, L., Vesela, K., Hansikova, H., Hulkova, H., Zeman, J., 2009. Loss of function of Sco1 and its interaction with cytochrome c oxidase. American Journal of Physiology - Cell Physiology 296(5):C1218—C1226.
[22] Sherwin, R.S., 1980. Role of the liver in glucose homeostasis. Diabetes Care 3(2):261—265.
[23] Chow, C.W., Thorburn, D.R., 2000. Morphological correlates of mitochondrial dysfunction in children. Human Reproduction 15(Suppl 2):68—78.
[24] Wiemerslage, L., Lee, D., 2016. Quantification of mitochondrial morphology in neurites of dopaminergic neurons using multiple parameters. Journal of Neuroscience Methods 262:56—65.
[25] Robinson, B.H., 2006. Lactic acidemia and mitochondrial disease. Molecular Genetics and Metabolism 89(1—2):3—13.
[26] Ress, C., Kaser, S., 2016. Mechanisms of intrahepatic triglyceride accumulation. World Journal of Gastroenterology 22(4):1664—1673.
[27] Legault, J.T., Strittmatter, L., Tardif, J., Sharma, R., Tremblay-Vaillancourt, V., Aubut, C., et al., 2015. A metabolic signature of mitochondrial dysfunction revealed through a monogenic form of Leigh Syndrome. Cell Reports 13(5):981—989.
[28] Fernandes, J., Saudubray, J., Van den Berghe, G., Walter, J.H., 2006. Disorders of mitochondrial fatty acid oxidation and related metabolic pathways. In: Inborn metabolic diseases, 4th ed. Wurzburg, Germany: Springer. p. 179.
[29] Wang, Y.X., 2010. PPARs: diverse regulators in energy metabolism and metabolic diseases. Cell Research 20(2):124—137.
[30] Macdonald, G.A., Bridle, K.R., Ward, P.J., 2001. Lipid peroxidation in hepatic steatosis in humans is associated with hepatic fibrosis and occurs predominantly in acinar zone (vol 16, pg 599, 2001). Journal of Gastroenterology and Hepatology 16(8), 953-953.
[31] Polakos, N.K., Cornejo, J.C., Murray, D.A., Wright, K.O., Treanor, J.J., Crispe, I.N., et al., 2006. Kupffer cell-dependent hepatitis occurs during influenza infection. American Journal Of Pathology 168(4):1169—1178 quiz 1404-1165.
[32] Tarasenko, T.N., Jestin, M., Matsumoto, S., Saito, K., Hwang, S., Gavrilova, O., et al., 2019. Macrophage derived TNFalpha promotes hepatic reprogramming to Warburg-like metabolism. Journal of Molecular Medicine (Berlin) 97:1231—1243.
[33] Baffy, G., 2009. Kupffer cells in non-alcoholic fatty liver disease: the emerging view. Journal of Hepatology 51(1):212—223.
[34] Bilzer, M., Roggel, F., Gerbes, A.L., 2006. Role of Kupffer cells in host defense and liver disease. Liver International 26(10):1175—1186.
[35] Brock, R.W., Lawlor, D.K., Harris, K.A., Potter, R.F., 1999. Initiation of remote hepatic injury in the rat: interactions between Kupffer cells, tumor necrosis factor-alpha, and microvascular perfusion. Hepatology 30(1):137—142.
[36] Hatano, M., Sasaki, S., Ohata, S., Shiratsuchi, Y., Yamazaki, T., Nagata, K., et al., 2008. Effects of Kupffer cell-depletion on concanavalin A-induced hepatitis. Cellular Immunology 251(1):25—30.
[37] Mori, I., Komatsu, T., Takeuchi, K., Nakakuki, K., Sudo, M., Kimura, Y., 1995. Viremia induced by influenza virus. Microbial Pathogenesis 19(4):237—244.
[38] Frankova, V., Rychterova, V., 1975. Inhalatory infection of mice with influenza A0/PR8 virus. II. Detection of the virus in the blood and extrapulmonary organs. Acta Virologica 19(1):35—40.
[39] Racanelli, V., Rehermann, B., 2006. The liver as an immunological organ. Hepatology 43(2 Suppl 1):S54—S62.
[40] Kakino, S., Ohki, T., Nakayama, H., Yuan, X., Otabe, S., Hashinaga, T., et al., 2018. Pivotal role of TNF-alpha in the development and progression of nonalcoholic fatty liver disease in a murine model. Hormone and Metabolic Research 50(1):80—87.
[41] Sturm, E., Havinga, R., Baller, J.F., Wolters, H., van Rooijen, N., Kamps, J.A., et al., 2005. Kupffer cell depletion with liposomal clodronate prevents suppression of Ntcp expression in endotoxin-treated rats. Journal of Hepatology 42(1):102—109.
[42] Tosello-Trampont, A.C., Landes, S.G., Nguyen, V., Novobrantseva, T.I., Hahn, Y.S., 2012. Kuppfer cells trigger nonalcoholic steatohepatitis development in diet-induced mouse model through tumor necrosis factor-alpha production. Journal of Biological Chemistry 287(48):40161—40172.
[43] Ye, J., Jiang, R., Cui, M., Zhu, B., Sun, L., Wang, Y., et al., 2014. Etanercept reduces neuroinflammation and lethality in mouse model of Japanese encephalitis. The Journal of Infectious Diseases 210(6):875—889.
[44] Shi, X.L., Zhou, W., Huang, H., Zhu, H.G., Zhou, P., Zhu, H.Y., et al., 2013. Inhibition of the inflammatory cytokine tumor necrosis factor-alpha with etanercept provides protection against lethal H1N1 influenza infection in mice. Critical Care 17(6).
[45] Kastl, L., Sauer, S.W., Ruppert, T., Beissbarth, T., Becker, M.S., Suss, D., et al., 2014. TNF-alpha mediates mitochondrial uncoupling and enhances

ROS-dependent cell migration via NF-kappa B activation in liver cells. FEBS Letters 588(1):175—183.

[46] Brealey, D., Karyampudi, S., Jacques, T.S., Novelli, M., Stidwill, R., Taylor, V., et al., 2004. Mitochondrial dysfunction in a long-term rodent model of sepsis and organ failure. American Journal of Physiology. Regulatory, Integrative and Comparative Physiology 286(3):R491—R497.

[47] Crouser, E.D., Julian, M.W., Morales, J., 2002. Cardiac dysfunction is associated with myocyte mitochondrial injury in a resuscitated model of acute bacterial sepsis. Critical Care Medicine 30(12). A53-A53.

[48] Gellerich, F.N., Trumbeckaite, S., Hertel, K., Zierz, S., Muller-Werdan, U., Werdan, K., et al., 1999. Impaired energy metabolism in hearts of septic baboons: diminished activities of Complex I and Complex II of the mitochondrial respiratory chain. Shock 11(5):336—341.

[49] Singer, M., 2007. Mitochondrial function in sepsis: acute phase versus multiple organ failure. Critical Care Medicine 35(9 Suppl):S441—S448.

[50] El-Khoury, R., Dufour, E., Rak, M., Ramanantsoa, N., Grandchamp, N., Csaba, Z., et al., 2013. Alternative oxidase expression in the mouse enables bypassing cytochrome c oxidase blockade and limits mitochondrial ROS overproduction. PLoS Genetics 9(1):e1003182.

[51] Gaude, E., Schmidt, C., Gammage, P.A., Dugourd, A., Blacker, T., Chew, S.P., et al., 2018. NADH shuttling couples cytosolic reductive carboxylation of glutamine with glycolysis in cells with mitochondrial dysfunction. Molecular Cell 69(4):581—593 e7.

[52] Mullen, A.R., Wheaton, W.W., Jin, E.S., Chen, P.H., Sullivan, L.B., Cheng, T., et al., 2012. Reductive carboxylation supports growth in tumour cells with defective mitochondria. Nature 481(7381):385—388.

[53] Fendt, S.M., Bell, E.L., Keibler, M.A., Olenchock, B.A., Mayers, J.R., Wasylenko, T.M., et al., 2013. Reductive glutamine metabolism is a function of the alpha-ketoglutarate to citrate ratio in cells. Nature Communications 4.

[54] Rajagopalan, K.N., Egnatchik, R.A., Calvaruso, M.A., Wasti, A.T., Padanad, M.S., Boroughs, L.K., et al., 2015. Metabolic plasticity maintains proliferation in pyruvate dehydrogenase deficient cells. Cancer & Metabolism 3:7.

[55] Downey, C., 2016. Serious infection during etanercept, infliximab and adalimumab therapy for rheumatoid arthritis: a literature review. International Journal of Rheumatic Diseases 19(6):536—550.

